Master's Degree in Physics of Complex Systems


Complex Networks

# Brain Network Analysis

*Author:* Daniel Montesinos Capacete
February 18, 2024

**Abstract**

This project explores the structural properties of a brain network using network tools for analysis. We look at different network aspects, like degree distribution, centrality quantities, small-world features, and community detection algorithms. We found, through our analysis, that the brain network exhibits characteristics of a small-world network. This makes good information processing possible thanks to high clustering and short average path lengths. Our community detection algorithms found clear groups within the network. The Louvain technique and greedy optimization algorithms gave us the most consistent results. Visualizing the network shows the interconnected nature of communities, with a clear center area where nodes exhibit high values of different centrality measures. Overall, our study gives a deeper understanding of how the brain network is ordered. We emphasize its complex but efficient design.

# Contents

# 1 Introduction

Over the last decades, the brain has been explored as a complex network, analyzed through graph theory [1, 2]. These brain networks are typically derived by applying various processing algorithms to the data obtained from magnetic resonance imaging (MRI)[3]. This approach has provided insights into various cognitive processes, including learning, intelligence or brain diseases [4, 5].

Using these networks, some studies have focused on investigating how cognitive training influences brain network organization, specifically in enhancing memory retrieval-based strategies [6]. Additionally, research into brain network integrity, particularly in the context of neurological disorders, have also been done [7, 8, 9].

The network that we are going to study represents neural interactions derived from MRI data of human patients using the Magnetic Resonance One-Click Pipeline (MROCP) [10]. Each node in this network corresponds to a voxel of neural tissue, while edges denote connections inferred from single fibers. Notably, a post-processing step retained only the largest connected component, eliminating noise and spurious connections. This real network that we are using is obtained from the Netzschleuder network repository [11]. All the code that I have use can be found at the following GitHub repository [12].

# 2 Methods

## 2.1 Network Measurements

In this section, we will explain the different measurements that we will obtain from the network in order to understand its structure. Throughout the rest of the text, $n$ refers to the total number of nodes in the graph, while $k_i$ corresponds to the degree of each node. To obtain the quantities discussed in this section, I will not consider the weights on my network in order to maintain a simple graph. All the definitions discussed here are taken from [13], and the vast majority of the coefficients will be computed using Networkx [14], unless otherwise stated.

### 2.1.1 Basic Analysis Measurements

- **Average clustering coefficient**: Also known as the Watts-Strogatz clustering coefficient, it quantifies how closely connected nearby nodes are in the network. Thus, it gives information about how often we can find local groups or cluster in the network. It is obtained using

$$\bar{C} = \frac{1}{n}\sum_i C_i = \frac{1}{n}\sum_i \frac{2t_i}{k_i(k_i-1)} \tag{1}$$

  where $C_i$ and $t_i$ are the clustering coefficient and number of transitive relations of node $i$ respectively.

- **Global clustering coefficient**: Also known as Newman transitivity, it measures how often sets of three connected nodes (triangles) appear within the network. Thus, cap-

tures the global clustering patterns in the graph. It is defines as

$$C = \frac{3|C_3|}{|P_2|}, \quad |C_3| = \frac{1}{6}\text{tr}(A^3), \quad |P_2| = \frac{1}{2}\sum_{i=1}^{N} k_i(k_i - 1) \tag{2}$$

where $|C_3|$ and $|P_2|$ are the total number of triangles and the total number of paths of length two of the network respectively.

- **Average Path length**: It is a measure of the typical distance, on average, between any two nodes when considering all possible shortest paths in the graph. This is, it is the average number of edges that must be visited to go from one node to another. if $d_{ij}$ is the shortest distance between the node $i$ and the node $j$, the average path length is obtained as

$$l = \frac{1}{n(n-1)}\sum_{i \neq j} d_{i,j}. \tag{3}$$

- **Diameter of the network**: The diameter $D$ of the network is defined as the longest shortest path between any pair of nodes within that network. This is, the diameter of the network correspond to $\max[\{d_{ij}\}_{i \neq j}]$.

- **Assortativity degree**: It is a measure that quantifies the preference of nodes in a network to attach to others with similar or dissimilar degrees. It is obtained as

$$r = \frac{\frac{1}{m}\sum_{(i,j)\in E} k_i k_j - \left(\frac{1}{2m}\sum_{(i,j)\in E}(k_i + k_j)\right)^2}{\frac{1}{2m}\sum_{(i,j)\in E}\left(k_i^2 + k_j^2\right) - \left(\frac{1}{2m}\sum_{(i,j)\in E}(k_i + k_j)\right)^2}. \tag{4}$$

  where $E$ is the set of edges within the graph.

- **Bipartivity index**: The bipartivity index quantifies how strongly a network exhibits a bipartite structure, where nodes can be divided into two distinct sets with edges only connecting nodes from different sets. A bipartivity index of one indicates a perfectly bipartite network, where there are no connections within the same set, while lower values suggest a decrease in the degree of bipartitivity, indicating more interconnections within the same set. It is computed as

$$b_e = \frac{\text{Tr}(\cosh(A)) - \text{Tr}(\sinh(A))}{\text{Tr}(\cosh(A)) + \text{Tr}(\sinh(A))} = \frac{\text{Tr}(\exp(-A))}{\text{Tr}(\exp(A))} \tag{5}$$

  where $A$ is the adjacency matrix of the graph. There is not a built-in function in NetworkX to calculate this coefficient, so I will code it myself.

### 2.1.2 Centrality Measurements

- **Degree centrality**: It assess the importance of a node within a network based on the number of links it has. This is, nodes with high degree centrality are those that are highly connected to other nodes. The Networkx function that I will be using normalize the degree centrality dividing by the maximum possible degree $k_{max} = n - 1$.

- **Closeness centrality**: It is a measure used to evaluate the centrality of a node based on its average distance to all other nodes. It quantifies how close a node is to all other nodes in the network. It is computed as the normalised inverse of the sum of topological distances in the graph:

$$CC(i) = \frac{n-1}{\sum_j d_{ij}}. \tag{6}$$

  High values of this centrality measurement indicate that those nodes are, on average, closer to all other nodes in the graph.

- **Betweenness centrality**: It is used to assess the importance of a node within a network based on its role in facilitating communication or information flow between other nodes. It quantifies the number of shortest paths that pass through a particular node. If $\rho(i,k,j)$ represents the number of shortest paths between nodes $i$ and $j$ that pass through node $k$, and $\rho(i,j)$ represents the total number of shortest paths between nodes $i$ and $j$, the betweenness centrality of a node is obtained as

$$BC(k) = \sum_{i \neq j \neq k} \frac{\rho(i,k,j)}{\rho(i,j)}. \tag{7}$$

- **Eigenvector centrality**: The eigenvector centrality of the node $i$ in a undirected, simple network is

$$\vec{\varphi}_1(i) = \left( \frac{1}{\lambda_1} A \vec{\varphi}_1 \right)_i \tag{8}$$

  where $\lambda_1$ is the greatest eigenvalue of the adjanccey matrix and $\vec{\varphi}_1$ is its corresponding eigenvector.

- **Katz index** The Katz centrality of the node $i$ in an undirected, simple network is defined as

$$K_i = \left( \left( \sum_{k=0}^{\infty} \alpha^k A^k \right) \cdot \overrightarrow{1} \right)_i = \sum_q \sum_j \varphi_j(i) \varphi_j(q) \frac{1}{1 - \alpha \lambda_j} \tag{9}$$

  where $\alpha$ is a free parameter and $\{\vec{\varphi}_j\}$ is the set of eigenvectors of the adjacency matrix. The second equality is true for $0 < \alpha < \lambda_1^{-1}$. This index evaluates a node's centrality by combining the influence of its nearby neighbors with that of nodes farther away, adjusted by the parameter $\alpha$. For this free parameter, I will compute $\lambda_1^{-1}$ and use $a = 0.5\lambda_1^{-1}$ which in my case yields $a = 0.012$.

- **Pagerank centrality**: It assesses the importance of a node in a network by considering the centrality of nodes that link to it. It was primarily applied to the world wide web, which is a directed network. In order to work with undirected graphs, we just need to assume that for each undirected edge, there are two directed edges. Then, the matrix $H$ is defined as:

$$H_{ij} = \begin{cases} 1/k_i^{\text{out}} & \text{if there is a link from } i \text{ to } j \\ 0 & \text{otherwise} \end{cases} \tag{10}$$

where $k_i^{out}$ is the number of edges pointing outside of the node $i$ in the directed graph. It is possible to turn the matrix $H$ into a row stochastic one, defining:

$$S = H + \vec{a}\left[(1/n)\overrightarrow{1}^T\right], \quad a_i = \begin{cases} 1 & \text{if } k_i^{\text{out}} = 0 \\ 0 & \text{otherwise} \end{cases} \tag{11}$$

Now, using a free parameter $\alpha$, we define a matrix $G$ as

$$G = \alpha S + \left(\frac{1-\alpha}{n}\right)\overrightarrow{1}\overrightarrow{1}^T. \tag{12}$$

I will use $\alpha = 0.85$ which is the default value in NetworkX . If $\overrightarrow{PR}$ is the left eigenvector of $G$ corresponding to the greatest eigenvalue, then the PageRank centrality of node $i$ is

$$PR(i) = \left(G^T\overrightarrow{PR}\right)_i. \tag{13}$$

- **Subgraph centrality**: The subgraph centrality of the node i in a directed or undirected, simple or weighted network is:

$$EE(i) = [exp(A)]_{ii}. \tag{14}$$

## 2.2 Random Network Models

### 2.2.1 Erdös-Rényi

In the Erdös-Rényi model, proposed in 1959, we start with $n$ isolated nodes. Subsequently, pairs of nodes are selected, and with a probability $p > 0$, a link is added between them. A random number, $r$, is generated uniformly between $[0, 1]$ for each pair of nodes, and if $p > r$, a link is added. Consequently, setting $p = 0$ results in a disconnected network, while $p = 1$ yields a complete graph.

We will generate this network using *erdos_renyi_graph* function from the Python library NetworkX [14]. In order to do this, we need to fix the total number of nodes $n$ of the Erdős-Rényi graph and the probability $p$ for edge creation. Since the idea is to create a random network to compare it with our real network, $n$ will be equal to the number of nodes in our real network. To choose a value for the probability, we will use that the expected number of edges in this network is

$$\bar{m} = \frac{n(n-1)}{2}p. \tag{15}$$

Then, we will set $p$ to the value that gives $\bar{m}$ equal to the total amount of edges in the real network. It can be seen that this is equivalent to dividing the edges of the real network by the possible maximum amount that could be in this network.

### 2.2.2 Barabási-Albert

In the Barabási-Albert model, proposed by Barabási and Albert in 1999, the degree distribution follows a power-law distribution. This means that the probability of finding a node with degree $k$ decays as a power law.

The random network is built as follows. First, we initialize the network with a small number of nodes, denoted as $n_0$. At each step of the algorithm, a new node $u$ is added to the network and connected to $m' \leq n_0$ existing nodes. The probability of attaching node $u$ to a node $v$ is proportional to the degree of $v$. Consequently, new nodes are more likely to attach to existing nodes with high degree, a process known as preferential attachment.

We will generate this network using the *barabasi_albert_graph* function from the Python library NetworkX [14]. In order to do this, we need to fix the total number of nodes $n$ of the Barabási-Albert graph and the amount $m'$ which is the number of edges to attach from a new node to existing nodes. Similarly to the Erdős-Rényi model, $n$ will be equal to the number of nodes in our real network. To choose a value for $m'$, we will use the value of the average degree in the real network.

## 2.3 Community Detection

Community detection in networks refers to the process of finding densely connected clusters of nodes, known as communities. Connections between nodes in different communities should be, in general, relatively sparse.

Measuring the quality of the communities within the network is crucial in order to validate the community detection algorithms. One commonly used measure is modularity, proposed by Girvan and Newman [15]. Modularity measures the degree to which the density of edges within communities surpasses the density anticipated in a random network. Therefore, a cohesive community should have a high value of modularity. If $n_C$ represents the number of communities, $m_r$ is the number of edges within the r-th community, and $V_r$ denotes the set of vertices within the r-th community, the modularity is obtained as [13]

$$Q = \sum_{r=1}^{n_C} \left[ \frac{m_r}{m} - \left( \frac{\sum_{j \in V_r} k_j}{2m} \right)^2 \right]. \tag{16}$$

Below is a brief explanation of the different community detection algorithms that I have used.

- **Clauset-Newman-Moore greedy modularity optimization**: This approach relies on maximizing the modularity of the network [16]. It begins by assigning each node to its own community. Then, it systematically combines pairs of communities to maximize modularity, iteratively merging those that lead to the greatest increase in modularity. This process continues until reaching a point where further improvement in modularity is not possible. We will be using the *greedy_modularity_communities* function from NetworkX.

- **Label propagation**: It operates by assigning each vertex in the network a unique label initially. It iteratively updates vertex labels based on the most common label among their neighbors, fostering consensus within connected groups of vertices. This process continues until a stable state is reached, where vertices within the same community tend to share the same label. In our case, we will use a semi-synchronous label propagation method [17] which is implemented in the *label_propagation_communities* function from NetworkX.

- **Louvain community detection**: It is a heuristic approach for extracting the community structure of a network based on modularity optimization [18]. It operates in two steps: initially, each node is assigned to its own community, and then, for each node, attempts are made to maximize the modularity gain by potentially moving the node to neighboring communities. If no positive gain is achieved, the node remains in its original community. In the second step, a new network is constructed with the nodes representing the communities found in the first step. The weights of the links between these new nodes are determined by summing the weights of the links between nodes in the respective communities. After completing this step, the algorithm can reapply the first step to create larger communities with enhanced modularity. These two steps are iteratively executed until no further modularity gain is achieved or the gain falls below a specified threshold. We will be using the *louvain_communities* function from NetworkX.

- **Infomap community detection**: It is a greedy stochastic search algorithm designed to minimize the map equation and detect two level and multilevel flow communities in networks [19]. In order to do this, we will use infomap python package.

Apart from modularity, we will also use the coverage and performance of the communities in order to address their quality. The coverage of a partition represents the proportion of edges within communities relative to the total number of edges in the graph. It quantifies how well the partition captures the internal structure of the network, highlighting the density of connections within each community. On the other hand, the performance of a partition measures the number of intra-community edges plus inter-community non-edges divided by the total number of potential edges. It evaluates the partition's ability to delineate distinct communities while minimizing connections between them, thereby providing insight into the overall quality and coherence of the partition.

In order to assess the similarity of communities obtained using different algorithms and evaluate their validity, I will employ the Normalized Mutual Information (NMI). NMI is a variant of Mutual Information scaled between 0 (indicating no mutual information) and 1 (reflecting perfect correlation). Implemented in scikit-learn for Python [1], NMI is calculated as

$$NMI(X,Y) = \frac{2I(X;Y)}{H(X) + H(Y)} \tag{17}$$

where $I(X;Y)$ represents the mutual information, and $H(X)$ and $H(Y)$ denote the entropy in the information theory sense.

# 3 Results

## 3.1 Network Measurements

We will use the principal component of the network, which has $n = 1088$ nodes and $m = 16606$ edges. From these values, we obtain that the density of the network is $\rho = 2.81 \cdot 10^{-2}$ and the average degree is $\bar{k} = 30.52$, with a standard deviation of $\sigma[k] = 33.89$. Thus, the values of the degrees are spread out over a wide range from the mean, as we will see later on in their distribution. These results are similar to those in [11] for the corresponding network, taking into account that we are using the principal component of the network.

The rest of the structural properties of the networks that are explained in Sec. 2.1.1 are shown in Tab. 1. The first thing that we notice is that the Watts-Strogatz clustering and the global clustering coefficients have similar values. The values are relatively large, indicating that there is a significant number of clusters globally and locally within our brain network. Nonetheless, later on, we will compare these values with random models in order to see if they are truly meaningful.

The average path length is quite short, taking into account that we are dealing with a network with an order of $10^3$ nodes. Furthermore, the diameter of the network is also small. In order to properly address whether these values are significantly smaller or not, we will compare them to the values obtained from the random networks model in Sec. 3.2.

The assortativity coefficient is non-zero and exhibits a relatively high value, suggesting that nodes tend to attach preferentially to others with a similar degree. We will further assess the significance of this result by comparing it to random models. Finally, examining the bipartivity index, it is evident that the network is not bipartite.

| $\bar{C}$ | $C$ | $l$ | $D$ | $r$ | $b_e$ |
|---|---|---|---|---|---|
| 0.541 | 0.462 | 3.844 | 10 | 0.396 | $7.376 \cdot 10^{-29}$ |

Table 1: Results for the network structural properties that were defined in Sec. 2.1.1.

Apart from these coefficients, one of the most important structural properties of the network is its degree distribution. In order to gain some theoretical insight into the degree distribution, several fits to known distributions have been done. The probability density functions (PDFs) that I have used, as well as their corresponding parameters, are described in App. A. In general, the degree distribution of real networks is known to be irregular [13]. Then, it will be convenient to perform these fits to the cumulative probability distributions (CDFs), which are usually smooth. We will perform this process for fitting both the PDF and the CDF of our degree distribution in order to see the differences.

The results obtained for the fits are illustrated in Fig. 1 and Fig. 2 for fitting the CDF and PDF, respectively. The parameters of the fits can be seen in Tab. 8 within App. B. Our brain network exhibits a skewed distribution with a heavy tail, characterized by a large number of nodes with low degrees and a small number of nodes with high degrees. Observing Fig. 1, we can see that the majority of the distributions are able to qualitatively describe the shape of our CDF. However, when examining the corresponding PDFs, only some of them properly approximate the degree distribution's shape. Among these, the log-normal and the inverse Gaussian distributions are the closest to the data points. Although they

reproduce the shape of the PDF quite well, it is noticeable on the CDF plot that they do not perfectly match the curve of our CDF, indicating noticeable differences. This highlights the difficulty of fitting a real network distribution: while it is possible to find distributions that qualitatively seem to match the data, it is quite complicated to find a distribution that perfectly describes both the PDF and CDF curves.

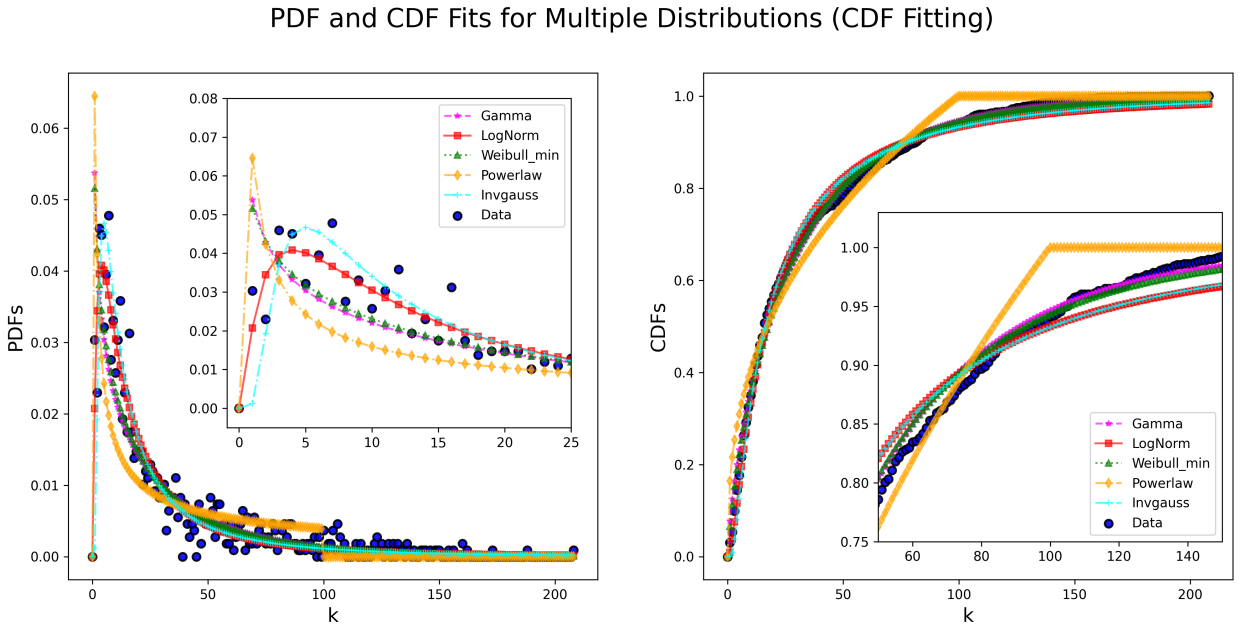


Figure 1: Fits for the degree distribution of our brain network. These results correspond to fitting the CDF.

On the other hand, looking at Fig. 2, it is possible to see how the distributions are now in general closer to the shape of the PDF as could be expected. However, looking on the left side at the CDF plot, this time most of the CDFs do not describe our CDF. It is interesting to note that the log-normal distribution is also performing quite well in both the PDF and CDF, even though is does not perfectly match the curve of the CDF as before. Furthermore, in Tab. 8, we can say that the parameters of the fit for the log-normal are almost the same when you fit the real PDF or CDF.

From this quick visual analysis, among the distributions we have tried, the log-normal distribution appears to better describe both distributions. To formally address this observation, I conducted the two-sample Kolmogorov-Smirnov test using scipy [20, 21]. The test results indicate that the only case in which the samples from the real network and the theoretical one are statistically indistinguishable with 95% confidence is for the log-normal distribution using the parameters obtained by fitting the CDF. Therefore, it can be concluded with high confidence that the statistical properties of our brain network degree distribution can be described by a log-normal distribution.

In real life, log-normal distributions commonly emerge in various phenomena, such as income distribution, stock prices, and sizes of natural phenomena like earthquakes and forest fires, reflecting multiplicative processes where growth or size accumulates proportionally [22].

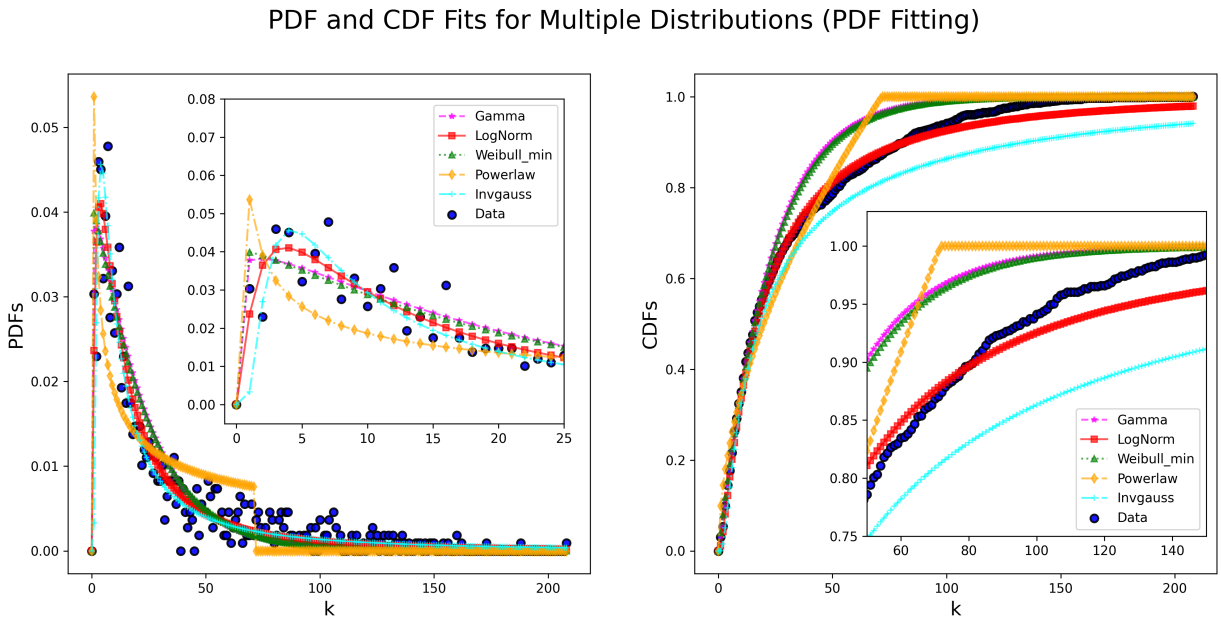


Figure 2: Fits for the degree distribution of our brain network. These results correspond to fitting the PDF.

Furthermore, there are biological mechanisms that could lead to a log-normal distribution [23]. For example, the log-normal distribution have been used to describe the statistically preserved firing rates and synaptic weights across brain states, explaining phenomena such as the similarity between spontaneous and evoked activity and the replay of waking neuronal sequences during sleep [24]. Therefore, it is not surprising to find a log-normal distribution in our brain network. In other studies where brain networks obtained from MRI scans of several patients were analyzed, a skewed degree distribution was also observed [25]. However, they suggest that the best distribution is a power law with a sharp cutoff, leading to a PDF of the form $f(x) \sim x^{\alpha-1}\exp(-x/x_{\text{crit}})$, which is a gamma distribution with some scaling, although they do not explicitly state it. In our case, the gamma distribution did not perform so well for our network, which might be due to differences in the processing algorithm used to obtain the brain network.

Finally, we are also going to study the most centrals nodes within our brain network according to the centrality measures defined in Sec. 2.1.2. The 25 nodes which have the highest value of the corresponding centrality measure are shown in Tab. 9 in App. B. The first thing we notice is that nodes 912 and 1016 rank very highly in all centrality measures. Furthermore, they are the first and second most central nodes for several of the centrality measures. In fact, all centrality measures share at least 70% of the nodes, except for betweenness centrality, which shares around 40%. This can be observed in Tab. 2, where the percentages of common nodes between different centrality measures are displayed. Closeness centrality is the one that has more common nodes with betweenness centrality (52%).

As explain in Sec. 2.1.2, betweenness centrality highlights nodes that play pivotal roles in connecting different parts of the network. The discrepancy between this centrality measure and the others suggests distinct roles for nodes in the network, indicating potential bridges

| | Degree Cent. | Clos. Cent. | Bet. Cent. | Eigen. Cent. | Katz Index | PageRank | Sub. Cent. |
|---|---|---|---|---|---|---|---|
| Degree Cent. | 100 | 88 | 48 | 84 | 92 | 88 | 84 |
| Clos. Cent. | 88 | 100 | 52 | 76 | 80 | 88 | 76 |
| Bet. Cent. | 48 | 52 | 100 | 40 | 44 | 48 | 40 |
| Eigen. Cent. | 84 | 76 | 40 | 100 | 92 | 72 | 100 |
| Katz Index | 92 | 80 | 44 | 92 | 100 | 80 | 92 |
| PageRank | 88 | 88 | 48 | 72 | 80 | 100 | 72 |
| Sub. Cent. | 84 | 76 | 40 | 100 | 92 | 72 | 100 |

Table 2: Percentage of common nodes among the top 25 nodes for the various centrality measures that have been used.

or bottlenecks. This implies that the network may exhibit specific structural characteristics that facilitate efficient information flow and communication pathways. This highlights the network's structural characteristics, potentially resembling a small-world network.

## 3.2 Comparison to Random Network Models

In this section, we will compare the previously obtained results with the Erdös-Rényi and Barabási-Albert random network models. These random models will serve as null hypotheses to assess whether the values for the different measures we obtained are statistically significant. In other words, we aim to determine whether the properties observed in our network stem from pure randomness or if they possess genuine biological significance. In order to perform this analysis, we will generate ten realizations of each of these random models using parameters that yield random networks with the same average degree as our real brain network.

### 3.2.1 Erdös-Rényi

In this case, we are going to generate Erdös-Rényi random networks using $p = 0.028$ and $n = 1088$ so they have the same amount of nodes and average degree as our network. The probability $p$ for adding edges is computed according to what is explained in Sec. 2.2.1. In each realization, we checked that the random network is connected.

The results for the coefficients that we previously studied within our brain network are shown in Tab. 3 for the random model. In the table, the average value with its corresponding standard deviation over the ten realizations is displayed. Comparing with Tab. 1, we can see that most of them are quite different from those in our brain network. The only ones that approximately coincide are the average path length, even though the one obtained in this random model is lower, and the bipartite index, which is practically zero in both cases. We observe that for this Erdős-Rényi network, both the global and average clustering coefficients are very small and have similar values. This is due to the fact that the probability for connecting edges is quite low. Nevertheless, the diameter of the network is smaller than the one that we obtain for our brain network. For this random model, we also get an assortativity which is practically zero, very different compared to the results from the real brain network.

Apart from this, we can also compare the degree distribution of the random model with the one obtained from the brain network. Both distributions are shown in Fig. 3. It is quite

| $\bar{C}$ | $C$ | $l$ | $D$ | $r$ | $b_e$ |
|---|---|---|---|---|---|
| $(2.796 \pm 0.034) \cdot 10^{-2}$ | $(2.794 \pm 0.032) \cdot 10^{-2}$ | $2.384 \pm 0.052$ | $3.20 \pm 0.40$ | $(-6.8 \pm 8.0) \cdot 10^{-4}$ | $(2.95 \pm 0.53) \cdot 10^{-8}$ |

Table 3: Results for the network structural properties of the Erdös-Rényi random model.

evident that the degree distribution obtained from the random model does not describe the brain network in any possible way. We see that the random model has a Poisson distribution with a peak around the average degree of our real network, as we could expect. However, it is clear that this distribution is totally different to our brain network, which is described by a log-normal distribution as we have seen.

Summarizing, none of the structural properties that we have discussed resembled those of the brain network. Therefore, the Erdős-Rényi model is unable to reproduce the properties of our real network, even though we are using parameters to match the number of nodes and average degree.

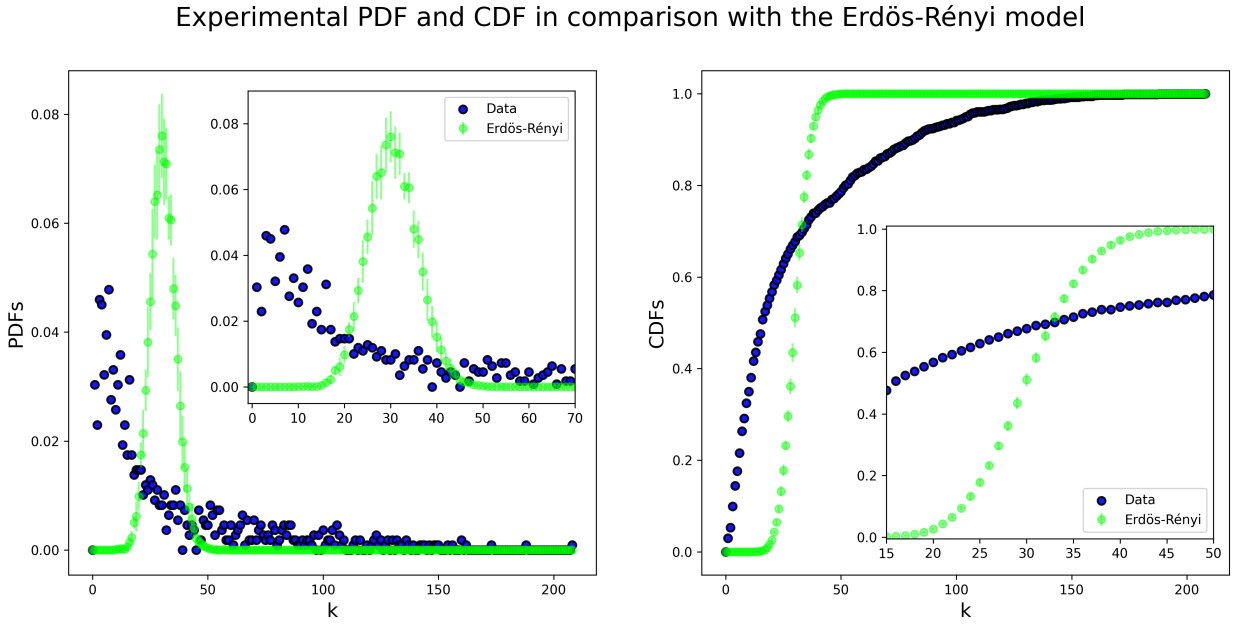


Figure 3: PDF and CDF of our brain network and the one obtained over ten realizations of the Erdös-Rényi model.

### 3.2.2 Barabási-Albert

In this case, we are going to generate Barabási-Albert random networks using $n = 1088$ and average degree $\bar{k} \approx 30$ so they have the same amount of nodes and average degree as our network. In each realization, we checked that the random network is connected.

The results for the coefficients that we previously studied within our brain network are shown in Tab. 4 for the random model. In the table, the average value with its corresponding standard deviation over the ten realizations is displayed. Comparing with Tab. 1, we can see that most of them are quite different from those in our brain network. Similarly to what

happened in the Erdös-Rényi model, the only coefficients that approximately coincide are the average path length, even though the one obtained in this random model is also lower, and the bipartite index, which is practically zero in both cases. We also have that both the global and average clustering coefficients of the random model are very small and have similar values. The diameter of the network is also smaller than the one that we obtain for our brain network as well as the assortativity which is practically zero, very different compared to the results from the real brain network.

| $\bar{C}$ | $C$ | $l$ | $D$ | $r$ | $b_e$ |
|---|---|---|---|---|---|
| $(1.171 \pm 0.016) \cdot 10^{-1}$ | $(1.1614 \pm 0.0078) \cdot 10^{-1}$ | $2.0135 \pm 0.0013$ | $3.0 \pm 0.0$ | $(-4.64 \pm 0.45) \cdot 10^{-3}$ | $(1.07 \pm 0.31) \cdot 10^{-29}$ |

Table 4: Results for the network structural properties of the Barabási-Albert random model.

In order to compare the degree distribution of the Barabási-Albert model with that of the brain network, both the PDFs and CDFs are shown in Fig. 3. In contrast to the Erdős-Rényi model, the degree distribution of the Barabási-Albert model exhibits an approximately similar shape to our brain network. Indeed, the CDFs exhibit closely matching curves. However, it does not entirely reproduce the PDFs for low values of the degree. This random model is known to exhibit a power-law degree distribution, as shown in Fig. 3. Thus, while our brain network shares some similarities in its degree distribution with a scale-free network, it cannot be considered as such due to clear differences in the PDFs.

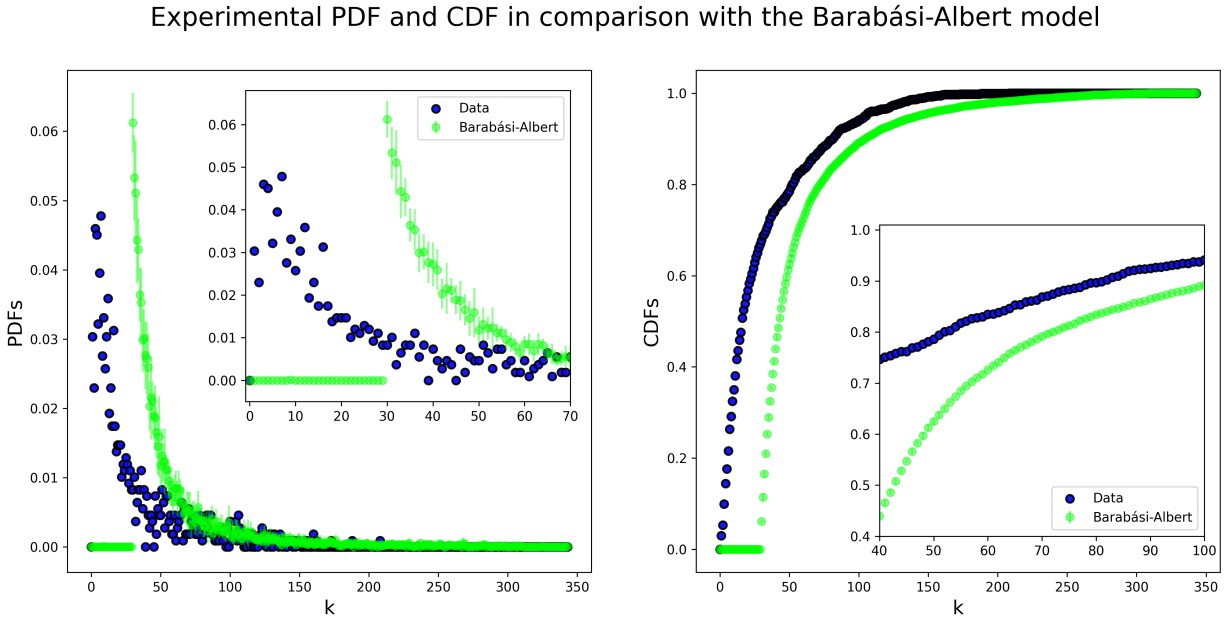


Figure 4: PDF and CDF of our brain network and the one obtained over ten realizations of the Barabási-Albert model.

In summary, none of the structural characteristics we examined closely mirrored those of the brain network. Although the degree distributions showed some similarities in certain regions, they did not precisely match those of our actual network. Consequently, the

Barabási-Albert model did not fully replicate the properties of our real network, even though we are using parameters to match the number of nodes and average degree.

### 3.2.3 Small World Network Analysis

A small-world network is characterized by high clustering, where nodes tend to form close groups, and short average path lengths, indicating that despite this clustering, the distance between any two nodes is relatively small [26]. They facilitate efficient communication via short paths, often described by the "six degrees of separation" phenomenon [27, 28]. They balance local clustering with global connectivity, sometimes featuring a scale-free structure resilient to random failures yet susceptible to targeted attacks due to highly connected nodes [29, 30]. They appear in may ways in real networks on different nature such as social, technological, transport and economic networks [31, 32]

Small-world networks emerge as an intermediate state between order and randomness. A small-world network, denoted as $n$, exhibits a high average cluster coefficient $\bar{C}_n$ alongside a low average path length $l_n$. However, determining what constitutes high or low values depends on the specific nature of the network under consideration. To address this, small-world networks are compared to a random network model $r$, which shares some characteristics with the original network. For a network to be classified as small-world, it must satisfy the following criteria [26, 33]

$$\lambda \equiv \frac{l_n}{l_r} \sim 1, \;\; \gamma \equiv \frac{\bar{C}_n}{\bar{C}_r} \gg 1, \;\; \sigma \equiv \frac{\gamma}{\lambda} > 1, \tag{18}$$

where $l_r$ and $C_r$ are the average path length and the average clustering coefficient for the corresponding random network. In our case, we are going to compute these coefficients using the Erdős-Rényi and Barabási-Albert models that we have just discussed. They both have the same number of nodes and average degree as our brain network. The results for these coefficients are shown in Tab. 5. The error is obtained using quadratic error propagation. As we can see, in both cases, the conditions for the small-world property are approximately satisfied. It is interesting to note that in the comparison with the Erdős-Rényi model, the values of $\gamma$ and $\sigma$ are notably larger.

| Random Model | $\lambda$ | $\gamma$ | $\sigma$ |
|---|---|---|---|
| Erdös-Rényi | $1.6108 \pm 0.0019$ | $19.32 \pm 0.29$ | $11.99 \pm 0.17$ |
| Barabási-Albert | $1.9096 \pm 0.0014$ | $4.597 \pm 0.062$ | $2.407 \pm 0.032$ |

Table 5: Coefficients to address the small world property for our brain network.

Looking at this analysis, we have that our brain network is indeed a small-world network. This is not surprising at all since small-worldness of brain networks has been extensively studied, derived from both structural and functional neuroimaging investigations [2, 33, 34, 35, 36, 37]. Furthermore, this property has been compared and associated with various neurophysiological disorders and conditions, including schizophrenia and Alzheimer's disease [38, 39]. Additionally, doing the same analysis as we have done here, diffusion-weighted MRI brain networks for several patients also satisfied the small-world network property [25].The

small-world topology is thought to contribute to reduced wiring costs and enhanced network efficiency within the brain, facilitating efficient communication via short paths while maintaining high clustering.

## 3.3 Community Detection

In this section, our aim is to search for communities within our brain network. To achieve this, we will employ various methods and quality measures as explained in Sec. 2.3. For the community detection tasks, we will use the network with the weight information, which was ignored in the previous analysis. The results obtained are summarized in Tab. 6, which shows the number of communities obtained and the corresponding modularity, coverage, and performance. It is important to note that the Louvain method may yield different results due to its dependence on the order of node consideration, so the algorithm is performed 100 times. In the table, we present the average value and the corresponding standard deviation.

Upon examining the results, we observe that the modularity is relatively high for the Louvain method and the greedy optimization algorithm. These modularity values can be considered acceptable evidence of communities in our network, considering the high clustering coefficients at both local and global scales, which can complicate finding a good partition. Moreover, since our brain network is a small-world network, finding communities may be challenging due to their dense internal connections and relatively strong connections to nodes outside the community. This is related to the high clustering and low average path length properties of small-world networks. This is noticeable in the label propagation and infomap algorithms, which yield significantly lower values of modularity. Indeed, the modularity obtained from the infomap detection algorithm is practically zero. The number of communities in this case is also very different from the rest. This means that these algorithms are just not performing well in our network, highlighting the importance of using several methods for community detection in networks.

Regarding coverage, we note that the maximum value is obtained for infomap, which also has the lowest modularity. This highlights the idea that communities are highly interconnected, and a partition with high coverage may result in low modularity values. Conversely, performance scores relatively high values compared to modularity and coverage. Specifically, the Louvain algorithm achieves the highest performance score while yielding the lowest coverage.

| Algorithim | $n_c$ | Modularity | Coverage | Performance |
|---|---|---|---|---|
| Greedy Optimization | 8 | 0.574 | 0.675 | 0.843 |
| Louvain | $9.36 \pm 0.76$ | $0.5958 \pm 0.0047$ | $0.622 \pm 0.019$ | $0.8742 \pm 0.0043$ |
| Label Propagation | 13 | 0.442 | 0.785 | 0.766 |
| InfoMap | 2 | 0.058 | 0.989 | 0.242 |

Table 6: Results of community detection algorithms are presented alongside modularity and quality measures.

To assess the similarity of different communities obtained from these algorithms, we use the NMI as explained in Sec. 2.3. The results for the NMI between the obtained communities are shown in Tab. 7. For the Louvain method, we only consider the communities with the

highest modularity out of the 100 realizations of the algorithm. In this case, the modularity was $Q = 0.604$. We observe that the NMI between the different partitions is relatively large only for the Louvain method and the greedy optimization algorithm, which have the largest NMI. Label propagation has lower values of the NMI, and the infomap's NMI is even lower.

| | Greedy Optimization | Label Propagation | Louvain |
|---|---|---|---|
| InfoMap | 0.322 | 0.289 | 0.276 |
| Louvain | 0.752 | 0.549 | - |
| Label Propagation | 0.547 | - | - |

Table 7: NMI comparisons between the partitions obtained from different community detection algorithms.

From these results, we can interpret that the label propagation and infomap methods are not performing well for our network. They yield significantly low values of modularity, and the communities they produce are quite different from those obtained by other algorithms, as evidenced by the low NMI. On the other hand, the Louvain and greedy optimization methods exhibit a relatively high NMI value and have a similar number of communities, which validates the results obtained from them.

## 3.4 Network Visualization

Finally, we will attempt to create a visually appealing plot of our brain network to illustrate the various properties discussed in the previous sections. To achieve this, I will use the computed properties from NetworkX and then transfer them to Cytoscape for visualization. Obtaining a nice plot was quite challenging since we are working with a network with 16606 edges. I chose to show the communities obtained from the Louvain method, which exhibits the highest modularity. Nonetheless, the most difficult part was to find an appropriate layout since the network itself did not have any position attribute. After trying several layouts, I decided to use the edge-weighted spring embedded layout, which is available in Cytoscape. This layout positions nodes to minimize forces between them, treating nodes as repelling physical objects connected by springs [40]. Apart from that, I created a binary edge attribute that can have a "same" or "mixed" value if it is connecting nodes from the same or different communities, respectively. I tried to add more features to the visualization using the shape of the nodes, the width and shape of the edges, the transparency of both edges and nodes. However, I did not see that it was really helping to visualize anything, rather making the plot more complicated to understand.

Using this approach, our brain network is displayed in Fig. 5. Two central communities are clearly identifiable in the middle of the network, surrounded by other communities. This central area can be referred to as the "center" of our brain network. Surrounding communities have nodes that are in close proximity to this center. The majority of edges connecting different communities are concentrated in this central area, as indicated by the high density of red-colored edges. Conversely, as we move away from the center, towards the periphery, we observe that most edges connect nodes within the same communities.

From this image, we can clearly observe the various properties that have been discussed throughout the project. It is clear that there is both global and local clustering, making

distinct communities that are relatively easy to spot. Additionally, there is extensive interconnection between these communities in the central area of the network, with fewer edges connecting different communities in the surroundings. This high level of interconnectivity leads to a low average path length despite the high clustering properties, consistent with the characteristics of a small-world network, as previously discussed.

Moreover, the central zone contains nodes with the highest value of the centrality measures. While this information is not directly evident in the visualization, applying filters in Cytoscape reveals that the central zone contains nodes with the highest values of the centrality measures. This finding aligns with expectations, as the central zone exhibits high connectivity among all communities, leading to elevated centrality in various measures. Consequently, the top 25 most central nodes were consistently similar across the majority of centrality measures at can be seen in Tab. 2. Additionally, these central nodes are highly interconnected, contributing to the positive, nonzero assortativity degree, indicating that nodes with high degrees tend to connect to other nodes with similarly high degrees.

Figure 5: Network visualization in which the color of the nodes represents the community obtained using the Louvain method. The color of the edges is light green for edges connecting nodes within the same community and dark red for edges connecting nodes from different communities. The size of the nodes is proportional to their degree.

# 4 Conclusions

In this study, we have explored different structural properties of a brain network derived from MRI data using graph theory. The degree distribution of our brain network exhibits a skewed shape with a heavy tail. It is best described by a log-normal distribution, as shown in Fig. 1 and Fig. 2. Comparing our network to the Erdös-Rényi and Barabási-Albert random models, we have demonstrated that they do not reproduce the structural properties of our network, such as the clustering coefficients, the average path length, the diameter, and assortativity degree. This highlights that the properties in our network do not arise from random processes, its structure comes from biological evolution. Furthermore, our analysis revealed a small-world structure within the brain network. As we have discussed, this is characterized by high clustering and short average path lengths. These findings align with existing literature discussed throughout the project, emphasizing that brain networks typically exhibit small-world characteristics.

Regarding community detection algorithms, the Louvain method and greedy optimization algorithm consistently obtaining similar communities, as shown in Table 7. Their modularity is quite high as can be seen in Tab. 6. Visualization of the brain network shows the interconnected nature of communities (see Fig. 5). There is a central zone in which all the nodes have high values of various centrality measures. In this central area, all communities are highly interconnected, leading to short average path lengths despite the high clustering. The code that I have use as well as the Cytoscape file can be found at the following GitHub repository [12].

Overall, the brain is a complex system that supports a wide range of functions, including tasks at local and global scale. Using network theory to understand this biological complexity has proven to be a powerful tool. The small-world network describing our brain's architecture plays a crucial role in enabling both local and coordinated processing across interconnected brain regions. This network structure facilitates efficient information transfer and robustness against random perturbations.

# A Probability Distributions

To perform the fitting of probability distribution functions (PDFs) and cumulative distribution functions (CDFs), I will utilize the *curve_fit* function available in Scipy [20]. Below are the distributions that will be employed for the fitting process.

- **Gamma**: $x \geq 0$, $a > 0$ and $\Gamma(a)$ is the gamma function

$$f(x, a) = \frac{x^{a-1} e^{-y}}{\Gamma(a)}. \tag{19}$$

- **Lognormal**: $x > 0$, $s > 0$

$$f(x, s) = \frac{1}{sx\sqrt{2\pi}} \exp\left(-\frac{\log^2(x)}{2s^2}\right). \tag{20}$$

- **Weibull minimum**: $x > 0$, $c > 0$

$$f(x, c) = cx^{c-1} exp(-x^c). \tag{21}$$

- **Powerlaw**: $1 \geq x \geq 0$, $a > 0$

$$f(x, a) = ax^{a-1} \tag{22}$$

- **Invgauss** $x \geq 0$, $a > 0$

$$f(x, \mu) = \frac{1}{\sqrt{2\pi x^3}} \exp\left(-\frac{(x-\mu)^2}{2x\mu^2}\right). \tag{23}$$

Apart from the corresponding shape parameter in each of them ($a$, $s$, $c$,...), I will also use the "scale" parameter that changes the variable to $x' = x/\text{scale}$. The PDF is properly renormalized by simply dividing it by the scale parameter; this functionality is already implemented in SciPy. For the power law distribution, this adjustment means that its domain will change to scale $\geq x \geq 0$.

# B Tables

| Distribution | $\text{Shape}_{CDF}$ | $\text{Scale}_{CDF}$ | $\text{Shape}_{PDF}$ | $\text{Scale}_{PDF}$ |
|---|---|---|---|---|
| Gamma | $0.703 \pm 0.011$ | $42.83 \pm 0.75$ | $1.089 \pm 0.037$ | $20.16 \pm 1.13$ |
| LogNorm | $1.194 \pm 0.012$ | $16.69 \pm 0.18$ | $1.235 \pm 0.022$ | $16.84 \pm 0.44$ |
| Weibull min | $0.8136 \pm 0.0064$ | $27.28 \pm 0.17$ | $1.027 \pm 0.024$ | $22.69 \pm 0.71$ |
| Powerlaw | $0.3919 \pm 0.0090$ | $99.7 \pm 1.8$ | $0.541 \pm 0.027$ | $71.6 \pm 5.1$ |
| Invgaus | $2.154 \pm 0.064$ | $15.21 \pm 0.36$ | $4.45 \pm 0.69$ | $12.56 \pm 0.42$ |

Table 8: Parameters obtained out of the fitting process for the degrre distribution. $\text{Shape}_{CDF}$ and $\text{Scale}_{CDF}$ refers to the values obtained by fitting the CDF. $\text{Shape}_{PDF}$ and $\text{Scale}_{PDF}$ refers to the values obtained by fitting the PDF

| Hierarchy | Degree Cent. | Clos. Cent. | Bet. Cent. | Eigen. Cent. | Katz Index | PageRank | Sub. Cent. |
|---|---|---|---|---|---|---|---|
| 1 | 912 | 912 | 529 | 912 | 912 | 912 | 912 |
| 2 | 1016 | 529 | 912 | 1016 | 1016 | 1016 | 1016 |
| 3 | 1111 | 659 | 260 | 909 | 1111 | 1111 | 909 |
| 4 | 780 | 780 | 1016 | 1026 | 909 | 780 | 1026 |
| 5 | 909 | 663 | 359 | 1111 | 1026 | 913 | 1111 |
| 6 | 1026 | 1016 | 780 | 1110 | 780 | 1026 | 1110 |
| 7 | 1110 | 517 | 663 | 1029 | 1110 | 909 | 1029 |
| 8 | 913 | 908 | 441 | 780 | 1029 | 1110 | 780 |
| 9 | 1029 | 1111 | 843 | 908 | 659 | 659 | 908 |
| 10 | 659 | 1026 | 438 | 659 | 913 | 908 | 659 |
| 11 | 908 | 913 | 1111 | 782 | 908 | 901 | 782 |
| 12 | 785 | 909 | 233 | 639 | 517 | 785 | 639 |
| 13 | 1037 | 1037 | 1048 | 783 | 785 | 529 | 783 |
| 14 | 517 | 1029 | 524 | 784 | 1037 | 1037 | 784 |
| 15 | 901 | 647 | 149 | 781 | 647 | 517 | 781 |
| 16 | 647 | 924 | 913 | 913 | 924 | 1029 | 913 |
| 17 | 529 | 804 | 374 | 660 | 660 | 647 | 660 |
| 18 | 660 | 1128 | 908 | 647 | 782 | 1128 | 647 |
| 19 | 924 | 512 | 358 | 517 | 639 | 660 | 517 |
| 20 | 663 | 785 | 785 | 924 | 663 | 664 | 924 |
| 21 | 782 | 639 | 804 | 785 | 901 | 663 | 785 |
| 22 | 639 | 660 | 659 | 663 | 783 | 347 | 663 |
| 23 | 1128 | 347 | 1037 | 347 | 784 | 898 | 347 |
| 24 | 347 | 1110 | 769 | 792 | 347 | 924 | 792 |
| 25 | 783 | 664 | 1026 | 1122 | 781 | 809 | 1122 |

Table 9: Top 25 nodes for the various centrality measures that have been used.

# References


[1] Cornelis J. Stam. "Modern network science of neurological disorders". In: *Nature Reviews Neuroscience* 15.10 (2014), pp. 683–695. ISSN: 1471-0048. DOI: 10.1038/nrn3801. URL: https://doi.org/10.1038/nrn3801.

[2] Ed Bullmore and Olaf Sporns. "Complex brain networks: graph theoretical analysis of structural and functional systems". In: *Nature Reviews Neuroscience* 10.3 (2009), pp. 186–198. ISSN: 1471-0048. DOI: 10.1038/nrn2575. URL: https://doi.org/10.1038/nrn2575.

[3] Jonathan Clayden. "Imaging connectivity: MRI and the structural networks of the brain". In: *Functional neurology* 28 (Oct. 2013), pp. 197–203. DOI: 10.11138/FNeur/2013.28.3.197.

[4] Jeff W Lichtman and Joshua R Sanes. "Ome sweet ome: what can the genome tell us about the connectome?" In: *Current Opinion in Neurobiology* 18.3 (June 2008), pp. 346–353. DOI: 10.1016/j.conb.2008.08.010.

[5] Olaf Sporns. *Networks of the Brain*. MIT Press, 2011.

[6] Kaustubh Supekar et al. "Neurocognitive modeling of latent memory processes reveals reorganization of hippocampal-cortical circuits underlying learning and efficient strategies". In: *Communications Biology* 4.1 (2021), p. 405. ISSN: 2399-3642. DOI: 10.1038/s42003-021-01872-1. URL: https://doi.org/10.1038/s42003-021-01872-1.

[7] Bruno M. de Brito Robalo et al. "Improved sensitivity and precision in multicentre diffusion MRI network analysis using thresholding and harmonization". In: *NeuroImage: Clinical* 36 (2022), p. 103217. ISSN: 2213-1582. DOI: https://doi.org/10.1016/j.nicl.2022.103217. URL: https://www.sciencedirect.com/science/article/pii/S2213158222002820.

[8] Yanpei Wang et al. "Altered resting functional network topology assessed using graph theory in youth with attention-deficit/hyperactivity disorder". In: *Progress in Neuro-Psychopharmacology and Biological Psychiatry* 98 (2020), p. 109796. ISSN: 0278-5846. DOI: https://doi.org/10.1016/j.pnpbp.2019.109796. URL: https://www.sciencedirect.com/science/article/pii/S0278584619304920.

[9] Esther M Boot et al. "Functional brain connectivity in young adults with post-stroke epilepsy". In: *Brain Communications* 5.6 (Oct. 2023), fcad277. ISSN: 2632-1297. DOI: 10.1093/braincomms/fcad277. eprint: https://academic.oup.com/braincomms/article-pdf/5/6/fcad277/53898995/fcad277.pdf. URL: https://doi.org/10.1093/braincomms/fcad277.

[10] William Gray Roncal et al. "MIGRAINE: MRI Graph Reliability Analysis and Inference for Connectomics". In: *2013 IEEE Global Conference on Signal and Information Processing*. 2013, pp. 313–316. DOI: 10.1109/GlobalSIP.2013.6736878.

[11] Tiago P. Peixoto. *The Netzschleuder network catalogue and repository*. https://networks.skewed.de/net/human_brains. Network: BNU1_0025864_2_DTI_DS01216. 2020. DOI: 10.5281/zenodo.7839981.

[12] Daniel Montesinos. *Jupyter Notebook*. Feb. 2024. URL: https://github.com/SrMontesinos01/Complex-Network-Project.

[13] Ernesto Estrada and Philip A. Knight. *A First Course in Network Theory*. English. United Kingdom: Oxford University Press, Mar. 2015. ISBN: 978-0-19-872645-6.

[14] Aric A. Hagberg, Daniel A. Schult, and Pieter J. Swart. "Exploring Network Structure, Dynamics, and Function using NetworkX". In: *Proceedings of the 7th Python in Science Conference*. Ed. by Gaël Varoquaux, Travis Vaught, and Jarrod Millman. Pasadena, CA USA, 2008, pp. 11–15. URL: https://www.osti.gov/biblio/960616.

[15] Mark Newman. *Networks: An Introduction*. USA: Oxford University Press, Inc., 2010. ISBN: 0199206651.

[16] Aaron Clauset, M. E. J. Newman, and Cristopher Moore. "Finding community structure in very large networks". In: *Phys. Rev. E* 70 (6 Dec. 2004), p. 066111. DOI: 10.1103/PhysRevE.70.066111. URL: https://link.aps.org/doi/10.1103/PhysRevE.70.066111.

[17] Gennaro Cordasco and Luisa Gargano. "Community Detection via Semi-Synchronous Label Propagation Algorithms". In: *CoRR* abs/1103.4550 (2011). arXiv: 1103.4550. URL: http://arxiv.org/abs/1103.4550.

[18] Vincent D Blondel et al. "Fast unfolding of communities in large networks". In: *Journal of Statistical Mechanics: Theory and Experiment* 2008.10 (Oct. 2008), P10008. DOI: 10.1088/1742-5468/2008/10/P10008. URL: https://dx.doi.org/10.1088/1742-5468/2008/10/P10008.

[19] Jelena Smiljanić and Christopher Blöcker. *Community Detection with the Map Equation and Infomap: Theory and Applications*. https://synthical.com/article/27d00c83-9b3d-43c0-9049-7b41a23a48dd. Oct. 2023. arXiv: 2311.04036 [physics.data-an].

[20] Pauli Virtanen et al. "SciPy 1.0: Fundamental Algorithms for Scientific Computing in Python". In: *Nature Methods* 17 (2020), pp. 261–272. DOI: 10.1038/s41592-019-0686-2.

[21] Joseph L. Hodges. "The significance probability of the smirnov two-sample test". In: *Arkiv för Matematik* 3 (1958), pp. 469–486. URL: https://api.semanticscholar.org/CorpusID:121451525.

[22] Eckhard Limpert, Werner A. Stahel, and Markus Abbt. "Log-normal Distributions across the Sciences: Keys and Clues: On the charms of statistics, and how mechanical models resembling gambling machines offer a link to a handy way to characterize log-normal distributions, which can provide deeper insight into variability and probability—normal or log-normal: That is the question". In: *BioScience* 51.5 (May 2001), pp. 341–352. ISSN: 0006-3568. DOI: 10.1641/0006-3568(2001)051[0341:LNDATS]2.0.CO;2. eprint: https://academic.oup.com/bioscience/article-pdf/51/5/341/26891292/51-5-341.pdf. URL: https://doi.org/10.1641/0006-3568(2001)051[0341:LNDATS]2.0.CO;2.

[23] Arthur L. Koch. "The logarithm in biology 1. Mechanisms generating the log-normal distribution exactly". In: *Journal of Theoretical Biology* 12.2 (1966), pp. 276–290. ISSN: 0022-5193. DOI: https://doi.org/10.1016/0022-5193(66)90119-6. URL: https://www.sciencedirect.com/science/article/pii/0022519366901196.

[24] György Buzsáki and Kenji Mizuseki. "The log-dynamic brain: how skewed distributions affect network operations". In: *Nat Rev Neurosci* 15.4 (Apr. 2014), pp. 264–278. DOI: 10.1038/nrn3687. URL: https://doi.org/10.1038/nrn3687.

[25] Yasser Iturria-Medina et al. "Studying the human brain anatomical network via diffusion-weighted MRI and Graph Theory". In: *NeuroImage* 40.3 (Apr. 2008), pp. 1064–1076. DOI: 10.1016/j.neuroimage.2007.10.060. URL: https://doi.org/10.1016/j.neuroimage.2007.10.060.

[26] Duncan J. Watts and Steven H. Strogatz. "Collective dynamics of 'small-world' networks". In: *Nature* 393.6684 (1998), pp. 440–442. ISSN: 1476-4687. DOI: 10.1038/30918. URL: https://doi.org/10.1038/30918.

[27] I. Samoylenko et al. "Why Are There Six Degrees of Separation in a Social Network?" In: *Phys. Rev. X* 13 (2 May 2023), p. 021032. DOI: 10.1103/PhysRevX.13.021032. URL: https://link.aps.org/doi/10.1103/PhysRevX.13.021032.

[28] Vito Latora and Massimo Marchiori. "Efficient Behavior of Small-World Networks". In: *Phys. Rev. Lett.* 87 (19 Oct. 2001), p. 198701. DOI: 10.1103/PhysRevLett.87.198701. URL: https://link.aps.org/doi/10.1103/PhysRevLett.87.198701.

[29] S. Havlin et al. "Vulnerability of network of networks". In: *The European Physical Journal Special Topics* 223.11 (2014), pp. 2087–2106. DOI: 10.1140/epjst/e2014-02251-6. URL: https://doi.org/10.1140/epjst/e2014-02251-6.

[30] Rui-qi Li et al. "Effect of clustering on attack vulnerability of interdependent scale-free networks". In: *Chaos, Solitons Fractals* 80 (2015). Networks of Networks, pp. 109–116. ISSN: 0960-0779. DOI: https://doi.org/10.1016/j.chaos.2015.06.022. URL: https://www.sciencedirect.com/science/article/pii/S0960077915001927.

[31] Xiao Fan Wang and Guanrong Chen. "Complex networks: small-world, scale-free and beyond". In: *IEEE Circuits and Systems Magazine* 3.1 (2003), pp. 6–20. DOI: 10.1109/MCAS.2003.1228503.

[32] Katherine A. Seaton and Lisa M. Hackett. "Stations, trains and small-world networks". In: *Physica A: Statistical Mechanics and its Applications* 339.3 (2004), pp. 635–644. ISSN: 0378-4371. DOI: https://doi.org/10.1016/j.physa.2004.03.019. URL: https://www.sciencedirect.com/science/article/pii/S0378437104003036.

[33] Mark D. Humphries, Kevin Gurney, and Tony J. Prescott. "The brainstem reticular formation is a small-world, not scale-free, network". In: *Proc Biol Sci* 273.1585 (2006), pp. 503–511. DOI: 10.1098/rspb.2005.3354.

[34] Danielle S. Bassett and Edward Bullmore. "Small-world brain networks". In: *Neuroscientist* 12.6 (2006), pp. 512–523. DOI: 10.1177/1073858406293182.

[35] Yong He, Zhi J. Chen, and Alan C. Evans. "Small-world anatomical networks in the human brain revealed by cortical thickness from MRI". In: *Cerebral Cortex* 17.10 (2007), pp. 2407–2419. DOI: 10.1093/cercor/bhl149.

[36] Olaf Sporns. "Contributions and challenges for network models in cognitive neuroscience". In: *Nature Neuroscience* 17.5 (2014), pp. 652–660. DOI: 10.1038/nn.3690.

[37] Danielle S. Bassett and Edward T. Bullmore. "Small-World Brain Networks Revisited". In: *Neuroscientist* 23.5 (2017), pp. 499–516. DOI: 10.1177/1073858416667720.

[38] Mary-Ellen Lynall et al. "Functional connectivity and brain networks in schizophrenia". In: *Journal of Neuroscience* 30.28 (2010), pp. 9477–9487. DOI: 10.1523/JNEUROSCI.0333-10.2010.

[39] Yong Liu et al. "Disrupted small-world networks in schizophrenia". In: *Brain* 131.Pt 4 (2008), pp. 945–961. DOI: 10.1093/brain/awn018.

[40] Tomihisa Kamada and Satoru Kawai. "An algorithm for drawing general undirected graphs". In: *Information Processing Letters* 31.1 (1989), pp. 7–15. ISSN: 0020-0190. DOI: https://doi.org/10.1016/0020-0190(89)90102-6. URL: https://www.sciencedirect.com/science/article/pii/0020019089901026.